Understanding the Improvement in the Electrochemical Properties of Surface Modified 5 V $LiMn_{1.42}Ni_{0.42}Co_{0.16}O_4$ Spinel Cathodes in Lithium-ion Cells

Jun Liu and Arumugam Manthiram*

Electrochemical Energy Laboratory & Materials Science and Engineering Program, The University of Texas at Austin, Austin, Texas 78712

Received January 2, 2009. Revised Manuscript Received February 28, 2009

The 5 V spinel cathode $LiMn_{1.42}Ni_{0.42}Co_{0.16}O_4$ with cation disorder in the 16d octahedral sites has been surface modified with 2 wt % nanosize Al_2O_3, ZnO, Bi_2O_3, and $AlPO_4$ by an electrostatic self-assembly method. The bare and surface-modified samples have been characterized by X-ray diffraction (XRD), Fourier transform infrared spectroscopy (FT-IR), high-resolution transmission electron microscopy (TEM), charge−discharge measurements in lithium cells, electrochemical impedance spectroscopy (EIS), and X-ray photoelectron spectroscopy (XPS). The surface-modified samples exhibit better cycling performance, better rate capability, and better rate capability retention during cycling compared to the bare sample. EIS and XPS studies show that the inferior electrochemical performances of the bare $LiMn_{1.42}Ni_{0.42}Co_{0.16}O_4$ are closely related to the formation of thick solid-electrolyte interfacial (SEI) layer at the high operating voltages of ∼5 V. Surface modifications with nanosize Al_2O_3, ZnO, Bi_2O_3, and $AlPO_4$ suppress the formation of thick SEI layers on $LiMn_{1.42}Ni_{0.42}Co_{0.16}O_4$ and thereby improve the electrochemical performances significantly. Moreover, the differences in the surface compositions formed during the annealing or electrochemical cycling processes also influence the electrochemical properties.

Introduction

Lithium-ion batteries are being intensively pursued for hybrid electric vehicle (HEV) and plug-in hybrid electric vehicle (PHEV) applications. Both the 4 V spinel $LiMn_2O_4$ and 3.4 V olivine $LiFePO_4$ have drawn much attention in this regard as Mn and Fe are inexpensive and environmentally benign, and they offer higher rate capability and better safety compared to the layered oxide cathodes. However, both $LiMn_2O_4$ and $LiFePO_4$ have limited energy density because of their low capacity or operating voltage. Considering the excellent intrinsic rate capability arising from the three-dimensional diffusion of lithium ions in the spinel lattice, one way to improve the energy and power densities is to increase the operating voltage. In this regard, cation-substituted spinel oxides $LiMn_{2-x}M_xO_4$ (M = Cr, Co, Fe, Ni, and Cu) are appealing as they deliver the capacity around a nearly flat operating voltage of ∼5 V.[1−8] The higher operating voltage is attributed to a binding of the M:3d e_g electrons by at least 0.5 eV higher than that of the Mn:3d e_g electrons.[9,10] Among the various 5 V spinel $LiMn_{2-x}M_xO_4$ cathodes investigated, $LiMn_{1.5}Ni_{0.5}O_4$ has drawn much attention because of its high capacity arising from the operation of $Ni^{2+/3+}$ and $Ni^{3+/4+}$ redox couples.[3,4]

However, the synthesis of $LiMn_{1.5}Ni_{0.5}O_4$ is often accompanied by the formation of $Li_xNi_{1-x}O$ impurity phase and is hampered by capacity fade. The capacity fade is believed to be due to the large lattice strain during cycling as it involves the formation of three cubic phases with a large lattice parameter difference during the charge−discharge process[11,12] and due to the corrosion reaction between the cathode surface and the electrolyte at the high operating voltage of ∼ 5 V.[13−16] Partial substitution of Mn and Ni in $LiMn_{1.5}Ni_{0.5}O_4$ by other elements like Li, Al, Mg, Ti, Cr, Fe, Co, Cu, Zn, and Mo have been pursued to improve the cyclability.[12,17−24] Some of these substitutions improve the

* Corresponding author. Phone: (512) 471−1791. Fax: (512) 471−7681. E-mail: rmanth@mail.utexas.edu.

(1) Sigala, C.; Guyomard, D.; Verbaere, A.; Piffard, Y.; Tournoux, M. *Solid State Ionics* **1995**, *81*, 167.
(2) Amine, K.; Tukamoto, H.; Yasuda, H.; Fujita, Y. *J. Electrochem. Soc.* **1996**, *143*, 1607.
(3) Amine, K.; Tukamoto, H.; Yasuda, H.; Fujita, Y. *J. Power Sources* **1997**, *68*, 604.
(4) Zhong, Q.; Bonakdarpour, A.; Zhang, M.; Gao, Y.; Dahn, J. R. *J. Electrochem. Soc.* **1997**, *144*, 205.
(5) Ein-Eli, Y.; Lu, S. H.; Rzeznik, M. A. *J. Electrochem. Soc.* **1998**, *145*, 3383.
(6) Ohzuku, T.; Takeda, S.; Iwanaga, M. *J. Power Sources* **1999**, *81*, 90.
(7) Strobel, P.; Ibarra Palos, A.; Anne, M.; Le Cras, F. *J. Mater. Chem.* **2000**, *10*, 429.
(8) Kim, J.-S.; Vaughey, J. T.; Johnson, C. S.; Thackeray, M. M. *J. Electrochem. Soc.* **2003**, *150*, A1498.
(9) Gao, Y.; Myrtle, K.; Zhang, M. J.; Reimers, J. N.; Dahn, J. R. *Phys. Rev. B: Condens. Matter.* **1996**, *54*, 16670.
(10) Obrovac, M. N.; Gao, Y.; Dahn, J. R. *Phys. Rev. B: Condens. Matter.* **1998**, *57*, 5728.
(11) Mukerjee, S.; Yang, X. Q.; Sun, X.; Lee, S. J.; McBreen, J.; Ein-Eli, Y. *Electrochim. Acta* **2004**, *49*, 3373.
(12) Arunkumar, T. A.; Manthiram, A. *Electrochem. Solid-State Lett.* **2005**, *8*, A403.
(13) Sun, Y. K.; Hong, K.-J.; Prakash, J.; Amine, K. *Electrochem. Commun.* **2002**, *4*, 344.
(14) Sun, Y. K.; Yoon, C. S.; Oh, I. H. *Electrochim. Acta* **2003**, *48*, 503.
(15) Alcántara, R.; Jaraba, M.; Lavela, P.; Tirado, J. L. *J. Electronal. Chem.* **2004**, *566*, 187.
(16) Noguchi, T.; Yamazaki, I.; Numataa, T.; Shirakata, M. *J. Power Sources* **2007**, *174*, 359.
(17) Arunkumar, T. A.; Manthiram, A. *Electrochim. Acta* **2005**, *50*, 5568.
(18) Ooms, F. G. B.; Kelder, E. M.; Schoonman, J.; Wagemaker, M.; Mulder, F. M. *Solid State Ionics* **2002**, *152*, 143.

10.1021/cm9000043 CCC: $40.75
Published on Web 03/27/2009

cyclability because of the stabilization of the spinel lattice with a disordering of the cations in the 16d octahedral sites and a smaller lattice parameter difference among the three cubic phases formed during cycling.[12] However, only a few groups have focused on improving the cyclability by suppressing the corrosion reaction via surface modification.[13−16] The surface modification of the 5 V spinels is limited mainly to ZnO[13−15] and Bi_2O_3,[16] whereas the surface modification of layered oxide have been pursued extensively with various coating materials including Al_2O_3 and $AlPO_4$.[25−34] We recently reported that the surface modification of the 5 V spinel $LiMn_{1.5}Ni_{0.42}Zn_{0.08}O_4$ with Al_2O_3, ZnO, and Bi_2O_3 leads to better cyclability, rate capability, and rate capability retention on cycling compared to the bare $LiMn_{1.5}Ni_{0.42}Zn_{0.08}O_4$.[35]

We found in our previous study[12] that a partial substitution of Mn and Ni by Co in $LiMn_{1.42}Ni_{0.42}Co_{0.16}O_4$ not only eliminates the formation of $Li_xNi_{1-x}O$ impurity, but also improves the rate capability with a much reduced lattice parameter difference among the three cubic phases formed during the charge−discharge process. We present here the surface modification of $LiMn_{1.42}Ni_{0.42}Co_{0.16}O_4$ by an electrostatic self-assembly method with nanosize Al_2O_3, ZnO, Bi_2O_3, and $AlPO_4$ and a characterization of the products by X-ray diffraction (XRD), Fourier transform infrared spectroscopy (FTIR), high-resolution transmission electron microscopy (TEM), electrochemical charge−discharge measurements, electrochemical impedance spectroscopy (EIS), and X-ray photoelectron spectroscopy (XPS). The characterization data are used to develop an in-depth understanding of the roles played by the solid-electrolyte interfacial (SEI) layer and the different nanosize surface modification layers on the electrochemical performances.

Experimental Section

$LiMn_{1.42}Ni_{0.42}Co_{0.16}O_4$ was synthesized by a hydroxide precursor method. The procedure involves the precipitation of the hydroxide precursors first from a solution containing required quantities of manganese, nickel, and cobalt acetates by adding KOH, followed by firing the oven-dried hydroxide precursor with a required amount of $LiOH \cdot H_2O$ at 900 °C in air for 12 h with a heating/cooling rate of 1 °C/min.

The nanosize Al_2O_3, ZnO, Bi_2O_3, and $AlPO_4$ were prepared by adding ammonium hydroxide (for Al_2O_3, ZnO, and Bi_2O_3) or $NH_4H_2PO_4$ (for $AlPO_4$) to the corresponding metal nitrate or acetate solutions. The pH values of the isoelectric point of Al_2O_3, ZnO, Bi_2O_3, and $AlPO_4$ have been reported to be, respectively, 9.2, 9.3, 7.6, and 4.7.[36−38] We measured the pH value of the isoelectric point of $LiMn_{1.42}Ni_{0.42}Co_{0.16}O_4$ to be ∼6 by a zeta potential analyzer (Zeta plus, Brookhaven Instruments Corporation). Accordingly, the coating of nanosize Al_2O_3, ZnO, Bi_2O_3, and $AlPO_4$ onto the spinel oxide surface was carried out by adjusting the pH of the solution containing a dispersion of the nanosize coating material to a value that is at the midpoint between the isoelectric points of the coating material and spinel $LiMn_{1.42}Ni_{0.42}Co_{0.16}O_4$ by adding acetic acid or ammonium hydroxide. After the pH was adjustinged to the desired value, the $LiMn_{1.42}Ni_{0.42}Co_{0.16}O_4$ powder was dispersed into the solution and stirred for half an hour at room temperature. Because the spinel $LiMn_{1.42}Ni_{0.42}Co_{0.16}O_4$ and the coating material have the opposite surface charges at the pH values chosen, the nanosize coating material self-assembled onto the surface of $LiMn_{1.42}Ni_{0.42}Co_{0.16}O_4$ by electrostatic attraction. The solution was then dried in an air-oven at ∼100 °C and the resulting mass was heated at 400−600 °C for 3 h. The amount of the nanosize coating material was controlled to be 2 wt %.

XRD patterns were recorded with a Phillips X-ray diffractometer with Cu Kα radiation between 10 and 90° at a scan rate of 0.01°/s. FTIR spectra were recorded with KBr pellets with a Perkin−Elmer IR spectrophotometer. The characteristic vibrational bands of the metal−oxygen bonds between 700 and 400 cm^{-1} were used to examine the ordering of cations in the 16d sites of the spinel lattice. The microstructures of the surface-modified samples were assessed with a JEOL 2010F TEM equipment.

Electrochemical performances were evaluated with CR2032 coin cells between 5.0 and 3.5 V. The coin cells were fabricated with the spinel oxide cathodes, metallic lithium anode, 1 M $LiPF_6$ in 1:1 diethyl carbonate/ethylene carbonate electrolyte, and Celgard polypropylene separator. The cathodes were prepared by mixing 75 wt % active material with 20 wt % conductive carbon and 5 wt % polytetrafluoroethylene (PTFE) binder, rolling the mixture into thin sheets, and cutting into circular electrodes of 0.64 cm^2 area.

The electrodes typically had an active material content of 6−8 mg. EIS data were collected with the bare and surface-modified $LiMn_{1.42}Ni_{0.42}Co_{0.16}O_4$ samples at 50% state of charge (SOC) with an ac amplitude of 10 mV in the frequency range of 10 kHZ to 50 mHZ and Li foil as both counter and reference electrodes.

XPS data were collected at room temperature with a Kratos analytical spectrometer and monochromatic Al Kα (1486.6 eV) X-ray source to assess the chemical state and concentration changes of the elements on the surface before and after cycling the cathode in lithium cells. Multiplex spectra of various photoemission lines were collected at medium resolution using an analyzer pass energy of 40 at 0.1 eV step and an integration interval of 1 s/eV. Sputtering was performed using an argon ion beam gun operating at 2 kV with a spot size of 2 × 2 mm^2. All spectra were calibrated with the C 1s photoemission peak at 285.0 eV to account for the charging effect.

(19) Hong, K.; Sun, Y. K. *J. Power Sources* **2002**, *109*, 427.
(20) Alcántara, R.; Jaraba, M.; Lavela, P.; Tirado, J. L.; Biensan, Ph.; Gulbert, A. de; Jordy, C.; Peres, J. P. *Chem. Mater.* **2003**, *15*, 2376.
(21) Fey, G. T. K.; Lu, C. Z.; Kumar, T. P. *J. Power Sources* **2003**, *115*, 332.
(22) Alcántara, R.; Jaraba, M.; Lavela, P.; Trado, J. L. *J. Electrochem. Soc.* **2004**, *151*, A53.
(23) Park, S. H.; Oh, S. W.; Myung, S. T.; Sun, Y. K. *Electrochem. Solid-State Lett.* **2004**, *7*, A451.
(24) Kim, J. H.; Myung, S. T.; Yoon, C. S.; Oh, I. H.; Sun, Y. K. *J. Electrochem. Soc.* **2004**, *151*, A1911.
(25) Cho, J.; Kim, Y. J.; Park, B. *Chem. Mater.* **2000**, *12*, 3788.
(26) Cho, J.; Kim, Y. J.; Park, B. *J. Electrochem. Soc.* **2002**, *149*, A1337.
(27) Liu, L.; Wang, Z.; Li, H.; Chen, L.; Huang, X. *Solid State Ionics* **2002**, *152−153*, 341.
(28) Chen, Z.; Dahn, J. R. *Electrochem. Solid-State Lett.* **2003**, *6*, A221.
(29) Cho, J.; Kim, Y. W.; Kim, B.; Lee, J. G.; Park, B. *Angew. Chem., Int. Ed.* **2003**, *42* (14), 1618.
(30) Cho, J.; Kim, T. G.; Kim, C.; Lee, J. G.; Kim, Y. W.; Park, B. *J. Power Sources* **2005**, *146*, 58.
(31) Appapillai, A. T.; Mansour, A. N.; Cho, J.; Yang, S.-H. *Chem. Mater.* **2007**, *19*, 5748.
(32) Cho, J.; Kim, Y. J.; Kim, T. J.; Park, B. *Angew. Chem., Int. Ed.* **2001**, *40*, 3367.
(33) Cho, J.; Kim, Y. J.; Park, B. *J. Electrochem. Soc.* **2001**, *148*, A1110.
(34) Chen, Z. H.; Dahn, J. R. *Electrochem. Solid-State Lett.* **2002**, *5*, A213−A216.
(35) Liu, J.; Manthiram, A. *J. Electrochem. Soc.* **2009**, *156*, A66.
(36) Bao, Y. H.; Nicholson, P. S. *J. Am. Ceram. Soc.* **2006**, *89*, 465–470.
(37) Parks, G. A. *Chem. Rev.* **1965**, *65*, 177.
(38) Williams, D. E.; Wright, G. A. *Electrochim. Acta* **1976**, *21*, 1009.

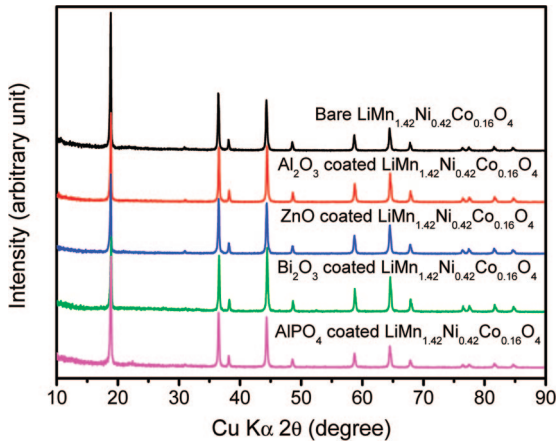

Figure 1. XRD patterns of the bare and 2 wt % Al_2O_3, ZnO, Bi_2O_3, and $AlPO_4$-coated $LiMn_{1.42}Ni_{0.42}Co_{0.16}O_4$.

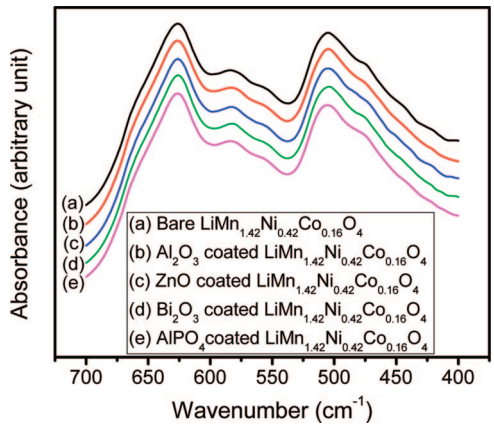

Figure 2. FTIR spectra of the bare and 2 wt % Al_2O_3, ZnO, Bi_2O_3, and $AlPO_4$-coated $LiMn_{1.42}Ni_{0.42}Co_{0.16}O_4$.

Results and Discussion

Structural and Microstructural Characterizations. XRD patterns of the bare and Al_2O_3, ZnO, Bi_2O_3, and $AlPO_4$-modified $LiMn_{1.42}Ni_{0.42}Co_{0.16}O_4$ are shown in Figure 1. All the reflections could be indexed on the basis of the cubic spinel structure, indicating that the surface modifications do not change the bulk structure of the spinel sample. The ordering of the cations in the 16d octahedral sites of the spinel $(Li)_{8a}[Mn_{1.5}Ni_{0.5}]_{16d}O_4$-based cathodes is known to influence significantly the electrochemical performances, especially the rate capability.[39] FTIR spectroscopy has been proven to be an effective technique in differentiating the ordered versus disordered structures of the $LiMn_{1.5}Ni_{0.5}O_4$-based cathodes.[40−42] The samples with cationic ordering are known to exhibit characteristic bands at 650, 465, and 430 cm^{-1} in the FTIR spectra. The absence of such bands in the FTIR spectra of both the bare and Al_2O_3, ZnO, Bi_2O_3, and $AlPO_4$-modified $LiMn_{1.42}Ni_{0.42}Co_{0.16}O_4$ in Figure 2 indicates that the cations are disordered in the 16d octahedral sites of $LiMn_{1.42}Ni_{0.42}Co_{0.16}O_4$ and the surface modifications do not cause any change in the cation disorder.

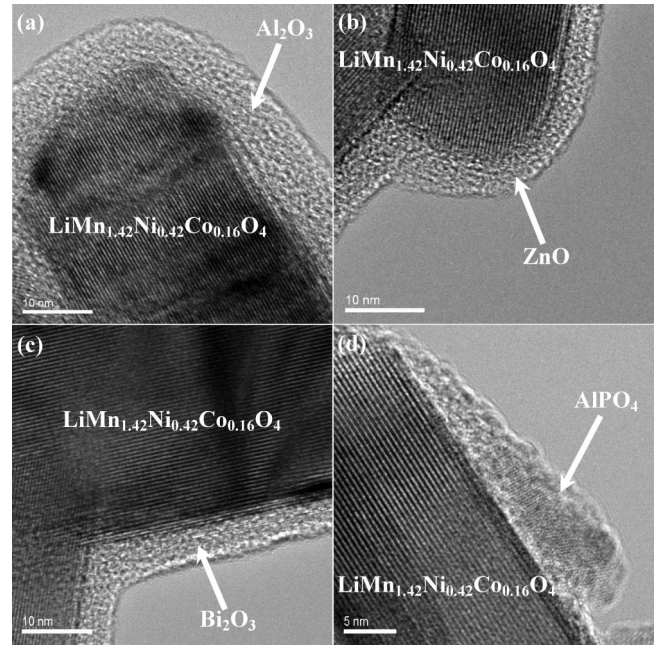

Figure 3. High-resolution TEM images of 2 wt % (a) Al_2O_3, (b) ZnO, (c) Bi_2O_3, and (d) $AlPO_4$-coated $LiMn_{1.42}Ni_{0.42}Co_{0.16}O_4$.

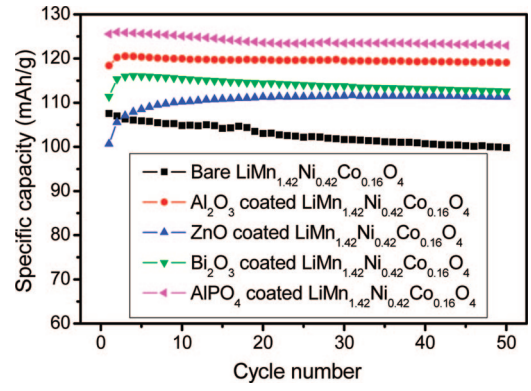

Figure 4. Cycling performances of the bare and 2 wt % Al_2O_3, ZnO, Bi_2O_3, and $AlPO_4$-coated $LiMn_{1.42}Ni_{0.42}Co_{0.16}O_4$.

Figure 3 shows the high-resolution TEM images of the Al_2O_3, ZnO, Bi_2O_3, and $AlPO_4$-modified $LiMn_{1.42}Ni_{0.42}Co_{0.16}O_4$ samples. The images indicate a coating of Al_2O_3, ZnO, Bi_2O_3, and $AlPO_4$ on the surface of the highly crystalline (as indicated by the fringe patterns) $LiMn_{1.42}Ni_{0.42}Co_{0.16}O_4$ spinel. Although Al_2O_3, ZnO, and Bi_2O_3 form a continuous, porous, amorphous (as indicated by the absence of fringe patterns) coating on $LiMn_{1.42}Ni_{0.42}Co_{0.16}O_4$, $AlPO_4$ forms a discrete, dense, crystalline (as indicated by the weak fringe pattern) coating. The TEM data demonstrate that the electrostatic self-assembly method is an effective way for surface modification.

Cycling Performance. Figure 4 compares the cycling performances of the bare and the surface modified $LiMn_{1.42}Ni_{0.42}Co_{0.16}O_4$. The bare $LiMn_{1.42}Ni_{0.42}Co_{0.16}O_4$ delivers a capacity of ∼108 mA h g^{-1} and exhibits a capacity retention of ∼93% in 50 cycles. All the surface modified samples show higher capacity and better capacity retention than the bare sample. The $AlPO_4$ modified $LiMn_{1.42}Ni_{0.42}$-

(39) Kim, J.-H.; Myung, S.-T.; Yoon, C. S.; Kang, S. G.; Sun, Y.-K. *Chem. Mater.* **2004**, *16*, 906.
(40) Alcantara, R.; Jaraba, M.; Lavela, P.; Trado, J. L.; Zhecheva, E.; Stoyanova, R. *Chem. Mater.* **2004**, *16*, 1573.
(41) Kunduraci, M.; Al-Sharab, J. F.; Amatucci, G. G. *Chem. Mater.* **2006**, *18*, 3585.
(42) Fang, H.; Li, L.; Li, G. *J. Power Sources* **2007**, *167*, 223.

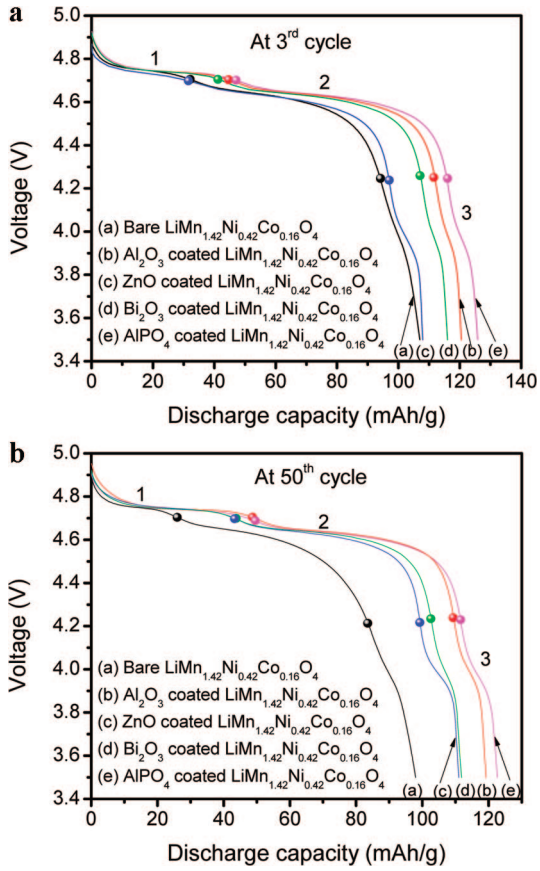

Figure 5. Comparison of the discharge profiles at (a) 3rd and (b) 50th cycles of $LiMn_{1.42}Ni_{0.42}Co_{0.16}O_4$ before and after coating with 2 wt % Al_2O_3, ZnO, Bi_2O_3, and $AlPO_4$. Discharge current density: 20 mA/g. The filled circles represent the separation points between different regions, which correspond to the points where the smallest absolute differential capacity value between the two neighboring peaks in differential capacity vs discharge voltage curves occurs.

$Co_{0.16}O_4$ delivers the highest capacity (~126 mA h g^{-1}) with a capacity retention of ~97% in 50 cycles, whereas the Al_2O_3-modified sample exhibits the best cyclability (~99% capacity retention in 50 cycles) with a capacity of ~120 mA h g^{-1}. Although our previous study[12] showed that the cation-substituted $LiMn_{1.42}Ni_{0.42}Co_{0.16}O_4$ exhibits better cyclability than the conventional $LiMn_{1.5}Ni_{0.5}O_4$, the surface modification of the former here offers further improvement in cyclability.

Figure 5 compares the discharge profiles at the third and 50th cycles of the bare and Al_2O_3, ZnO, Bi_2O_3, and $AlPO_4$-modified $LiMn_{1.42}Ni_{0.42}Co_{0.16}O_4$. All profiles exhibit three discharge plateaus as marked with the numbers 1, 2, and 3 and break points in Figure 5. The two plateaus around 4.7 V are due to the reduction of Ni^{4+} to Ni^{2+} and that around 4.0 V stems from the reduction of Mn^{4+} to Mn^{3+}.[31]

Table 1 gives the discharge capacity values observed in the three regions at the third and 50th cycles for the bare and surface modified samples. Comparison of the capacity values at the third and 50th cycles reveals that the observed capacity fade of the bare $LiMn_{1.42}Ni_{0.42}Co_{0.16}O_4$ sample is mainly due to the capacity decay in region 1 (the highest voltage region), and the surface modifications significantly improve the capacity retention in region 1. Previous study[12] has shown that the phase transition occurring in region 1 involves the largest lattice parameter change during the charge−discharge process. Also, region 1 corresponds to the highest voltage region. Therefore, one may envision that both the lattice stress caused by the large lattice parameter change and the corrosion reaction caused by electrolyte decomposition occurring at the high charge−discharge voltages may contribute to the capacity fade in region 1. Cho et al.[25,32] attributed the improved cycling performance of the oxide coated layered oxide cathodes to the increased fracture toughness of the coating oxides, which could suppress the lattice stress by constraining the cathode particles against the lattice parameter changes. On the other hand, Dahn et al.[34] have pointed out that the coating cannot suppress the lattice parameter changes of the layered oxide cathodes and the improvement in cycling performance is independent of the fracture toughness of the coating oxides. Similarly, Appapillai et al.[31] suggested that the better cycling performance of the $AlPO_4$-coated layered oxide cathodes compared to the bare sample is largely due to the differences in the surface microstructure rather than structural instability.

To differentiate these possibilities for the 5 V spinel cathodes, we examined the bare and surface modified electrodes by ex situ XRD at four different voltages on the discharge profiles: 4.9 V (the fully charged state), 4.7 V (the end point of region 1), 4.3 V (the end point of region 2), and 3.5 V (the fully discharged state). The lattice parameter values at the different discharge voltages were obtained by the Rietveld analysis of the XRD data. We found that the lattice parameters for the bare and the surface modified samples were similar at the various discharge voltages, indicating that the surface modification does not suppress the lattice parameter changes of the 5 V spinel during the charge−discharge process. Therefore, we can conclude that the improvement in the capacity values and capacity retention on going from the bare cathode to the surface modified cathode may be related to the suppression of the corrosion reaction caused by the electrolyte decomposition on cathode surface. This will be further discussed later with the EIS and XPS data.

Rate Capability and Rate Capability Retention. Rate capability of cathode materials is an important issue in judging their potential for high power applications. Accordingly, the rate capabilities of the bare and surface-modified samples were assessed after 3 and 50 cycles. Figure 6 compares the discharge profiles of the bare and Al_2O_3-coated $LiMn_{1.42}Ni_{0.42}Co_{0.16}O_4$ at various *C* rates after 3 and 50 cycles. To illustrate the differences in a better manner between the bare and coated samples, we normalized the discharge capacity values at various *C* rates to the discharge capacity value at a *C*/6 rate and plotted in panels a and b in Figure 7 for the bare and Al_2O_3, ZnO, Bi_2O_3, and $AlPO_4$-modified samples. As seen in Figure 7a, the surface modified samples show rate capabilities similar to the bare sample after 3 cycles except that the Bi_2O_3-coated sample exhibits slightly better rate capability. In contrast, all the surface-modified samples exhibit significantly much better rate capabilities than the bare samples after 50 cycles as seen in Figure 7b, and the rate capability increases in the order bare sample < $AlPO_4$-coated sample < ZnO-coated sample < Al_2O_3-coated sample < Bi_2O_3-coated sample. A comparison of the data in panels

Table 1. Discharge Capacities of the Bare and Surface-Modified (2 wt %) $LiMn_{1.42}Ni_{0.42}Co_{0.16}O_4$ in Different Regions at 3rd and 50th Cycles

	discharge capacity (mA h g^{-1}) at 3rd cycle			discharge capacity (mA h g^{-1}) at 50th cycle		
sample	region 1	region 2	region	region 1	region 2	region 3
bare $LiMn_{1.42}Ni_{0.42}Co_{0.16}O_4$	34.0	62.0	11.0	25.0	60.4	12.6
Al_2O_3-coated $LiMn_{1.42}Ni_{0.42}Co_{0.16}O_4$	44.4	68.1	8.0	44.7	64.9	9.6
ZnO-coated $LiMn_{1.42}Ni_{0.42}Co_{0.16}O_4$	36.0	62.1	9.8	42.7	58.2	11.7
Bi_2O_3-coated $LiMn_{1.42}Ni_{0.42}Co_{0.16}O_4$	42.6	65.2	8.2	41.9	61.0	8.9
$AlPO_4$-coated $LiMn_{1.42}Ni_{0.42}Co_{0.16}O_4$	47.7	68.7	9.4	45.2	66.4	11.0

a and b in Figure 7 indicates that the difference in rate capability between the surface-modified and the bare samples becomes increasingly significant as the cathodes are cycled (i.e. as the cycle number increases).

The rate capability as the cathodes are cycled is also an important parameter for practical applications. However, little attention has been paid in the literature to such studies. For simplicity, we present here the change in rate capability on cycling the cathode as "rate capability retention" in Figure 7c. The rate capability retention is defined as the ability to retain the rate capability on cycling, and the rate capability retention values are calculated here as the percentage ratio of the rate capability measured after 50 cycles to that measured after 3 cycles. In other words, the rate capability retention in Figure 7c was obtained by first calculating the percentage capacity retained on going from *C*/6 to various *C* rates (up to a 10*C* rate) at third and 50th cycles separately and then dividing the latter by the former. The data in Figure 7c demonstrate clearly that the rate capability retention increases significantly on surface modification of $LiMn_{1.42}Ni_{0.42}Co_{0.16}O_4$, and the rate capacity retention increases in the order bare sample < $AlPO_4$-coated sample < ZnO-coated sample < Bi_2O_3-coated sample < Al_2O_3-coated sample.

Polarization Behavior. Polarization resistance can play a significant role on the rate capability, as has been pointed

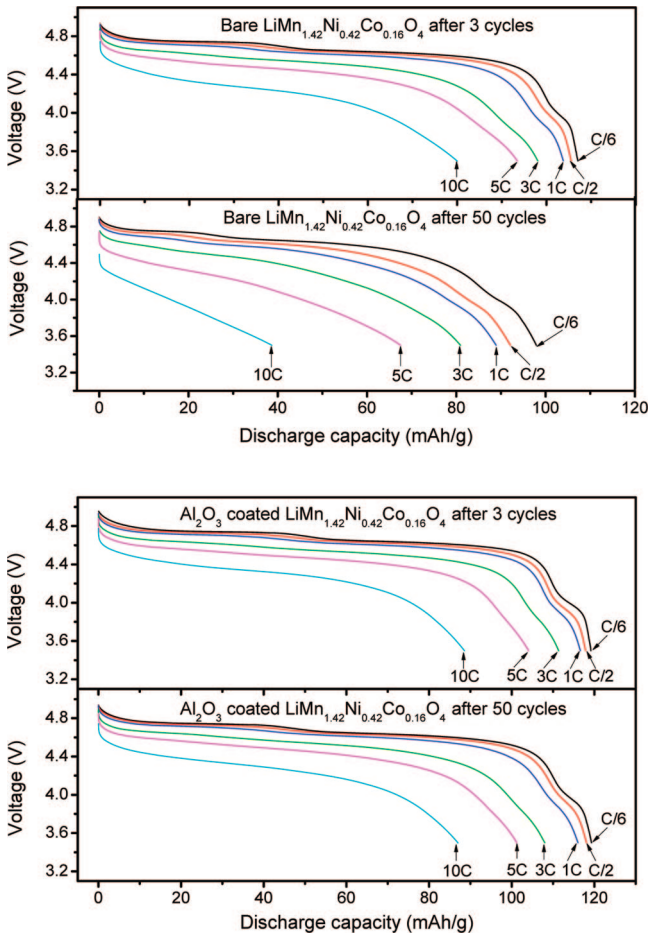

Figure 6. Discharge profiles illustrating the rate capabilities of bare and 2 wt % Al_2O_3-coated $LiMn_{1.42}Ni_{0.42}Co_{0.16}O_4$ after 3 and 50 cycles. Charge current density: 20 mA/g.

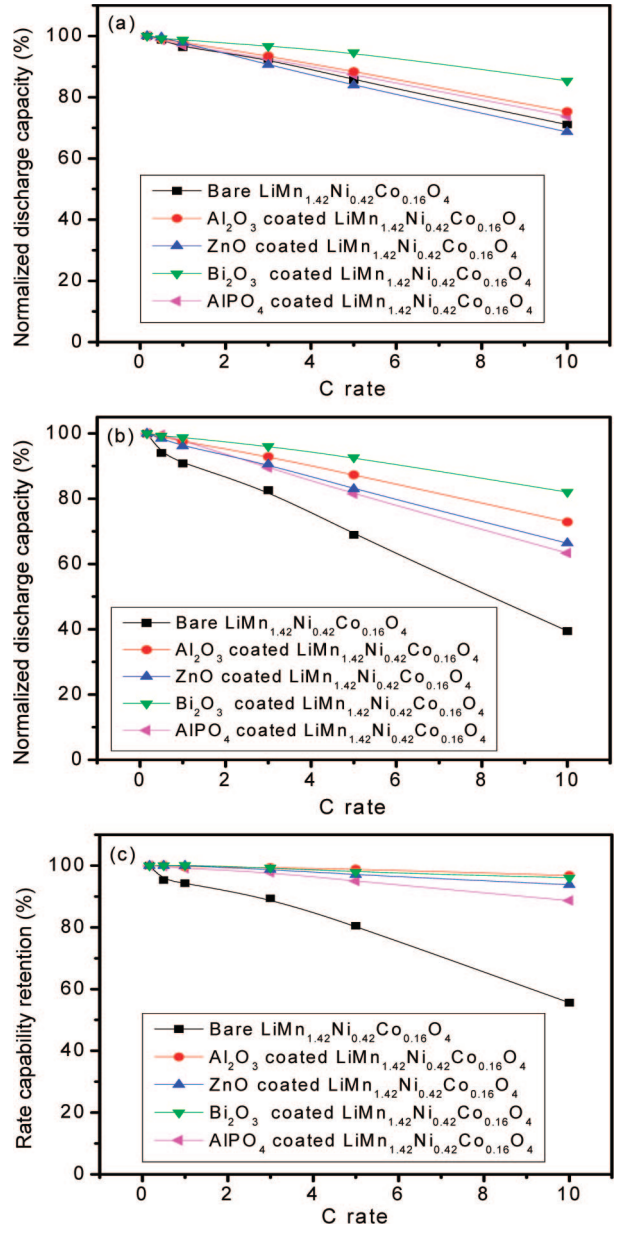

Figure 7. Comparison of the rate capabilities and rate capability retentions of $LiMn_{1.42}Ni_{0.42}Co_{0.16}O_4$ before and after coating with 2 wt % Al_2O_3, ZnO, Bi_2O_3, and $AlPO_4$: (a) normalized discharge capacity at 3rd cycle, (b) normalized discharge capacity at 50th cycle, and (c) rate capability retention (see the text for description).

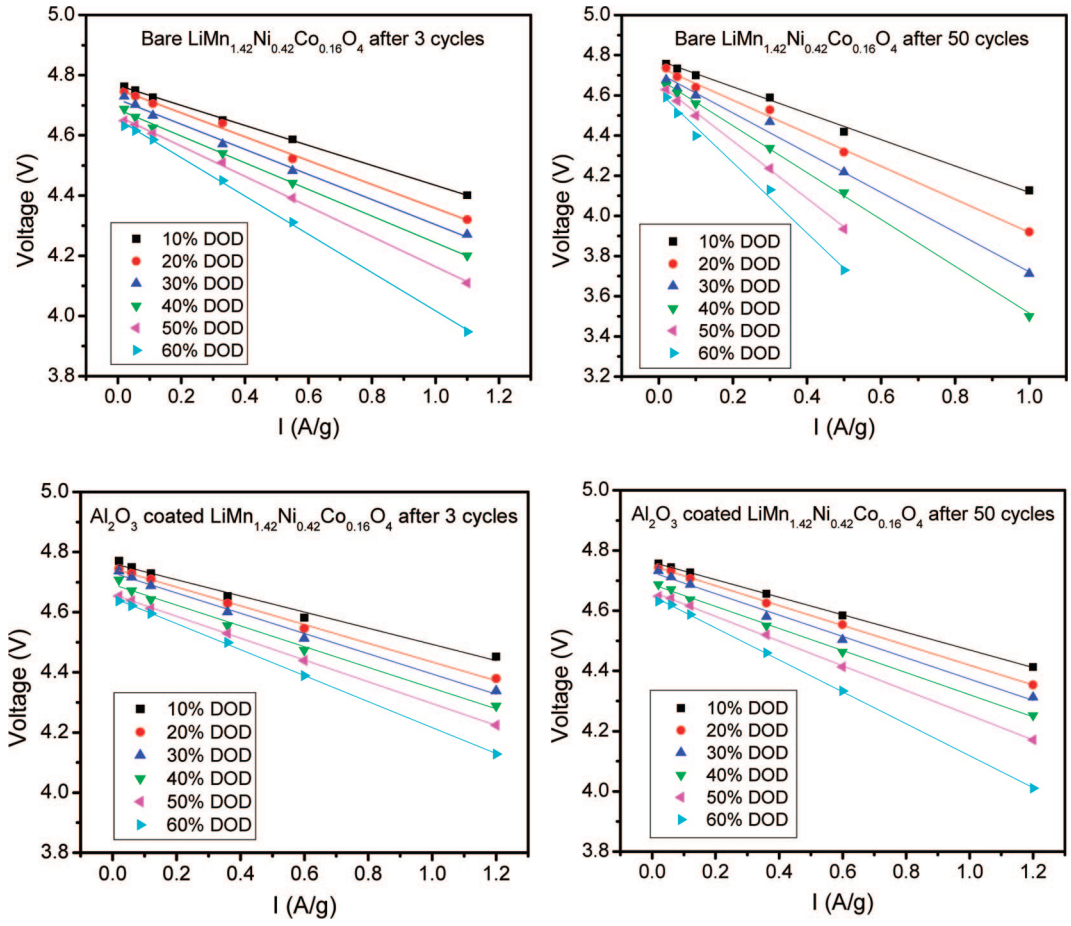

Figure 8. Relationship between voltage and current density at different depth of discharge (DOD) for 2 wt % Al_2O_3-coated $LiMn_{1.42}Ni_{0.42}Co_{0.16}O_4$ at (a) 3rd cycle and (b) 50th cycle.

out in the case of olivine $LiMnPO_4$.[43] To develop a relation between the rate capability and the total polarization resistance R_P, the discharge profiles at different discharge rates (see Figure 6) were analyzed further for the bare and various surface modified samples. On the basis of the relation $R_P = V/I$, the R_P value can be obtained from the voltage (V) vs mass current (I) curve in the domain where the voltage bears a linear relationship with current. Figure 8 shows the voltage vs mass current curves for the bare and Al_2O_3-modified $LiMn_{1.42}Ni_{0.42}Co_{0.16}O_4$. The data in Figure 8 indicate that the linear domain ranges from 10 to 60% depth of discharge (DOD), and the R_P values can be extracted from the slopes of these curves. It should be mentioned that the R_P values obtained here represents the total polarization resistance of the cell, which consists of the polarization resistances of the spinel cathode and the Li foil anode, the separator resistance, and the electrolyte resistance. Because the Li foil anode, separator, and electrolyte are identical for all cells, the polarization resistances induced by the Li foil anode, separator, and electrolyte can be assumed to be identical for all cells. Thus, the R_P obtained from the plots in Figure 8 can be used as an index to compare the polarization resistances of the bare and the surface-modified spinel cathodes.

Panels a and b in Figure 9 plot the R_P values versus DOD for the bare and the surface modified samples after 3 and 50 cycles. As seen, the R_P value increases with increasing DOD, which indicates that the kinetics of the discharge reaction becomes more and more unfavorable during the lithium insertion process. As seen in Figure 9a, the R_P value increases in the order Bi_2O_3-coated sample < Al_2O_3-coated sample < $AlPO_4$-coated sample < bare sample < ZnO-coated sample after 3 cycles, which is exactly the reverse order of the rate capability measured after 3 cycles in Figure 7a. Similarly, the R_P value increases in the order Bi_2O_3-coated sample < Al_2O_3-coated sample < $AlPO_4$-coated sample < ZnO-coated sample < bare sample as seen in Figure 9b, which is also in the reverse order of the rate capability data obtained after 50 cycles in Figure 7b. The increase in R_P on going from third to 50th cycle, which is termed as ΔR_P, is plotted versus DOD in Figure 9c. Interestingly, the order of ΔR_P is also exactly the reverse order of the rate capability retention in Figure 7c. The results indicate that the surface chemical stability increases in the order bare sample < $AlPO_4$-coated sample < ZnO-coated sample < Bi_2O_3-coated sample < Al_2O_3-coated sample.

Normally, R_P consists of three components: ohmic resistance R_Ω, activation resistance (also termed as charge transfer resistance) R_{ct}, and diffusion resistance R_d. The reason for the differences in the R_P and ΔR_P values of the various

(43) Delacourt, C.; Laffont, L.; Bouchet, R.; Wurm, C.; Leriche, J.-B.; Morcrette, M.; Tarascon, J.-M.; Masquelier, C. *J. Electrochem. Soc.* **2005**, *152*, A913.

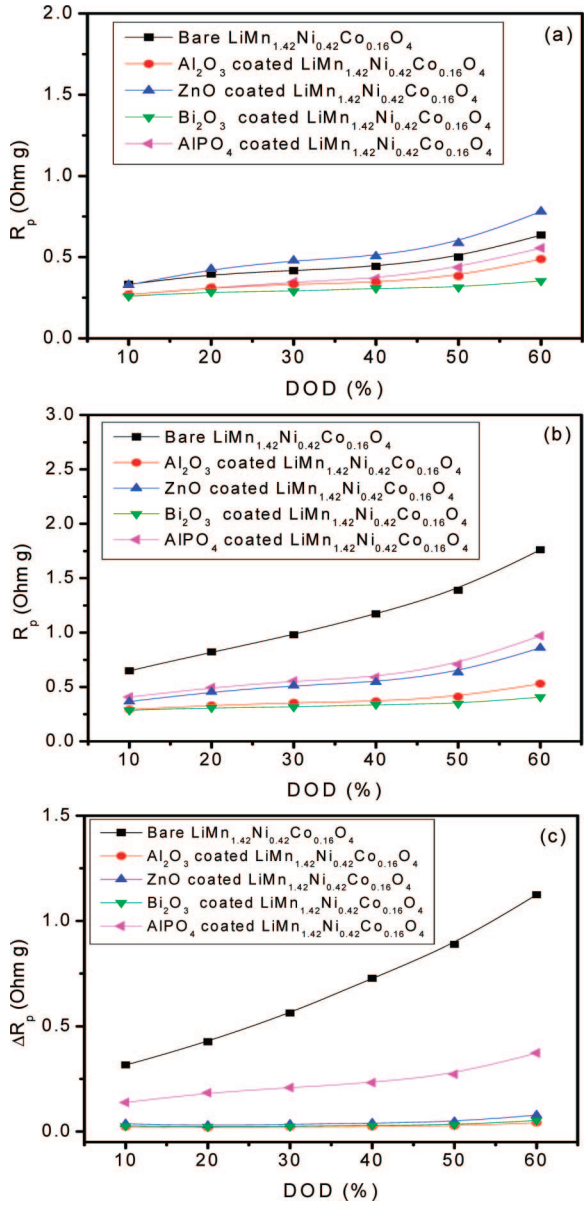

Figure 9. Variations of the polarization resistance (R_P) with depth of discharge (DOD) for the bare and 2 wt % Al_2O_3, ZnO, Bi_2O_3, and $AlPO_4$-coated $LiMn_{1.42}Ni_{0.42}Co_{0.16}O_4$ at (a) 3rd cycle and (b) 50th cycle. (c) Variations of ΔR_P (increase in R_P on going from 3rd to 50th cycle) with depth of discharge for the bare and 2 wt % Al_2O_3, ZnO, Bi_2O_3, and $AlPO_4$-coated $LiMn_{1.42}Ni_{0.42}Co_{0.16}O_4$.

samples can be identified from electrochemical impedance studies presented below.

Electrochemical Impedance Spectroscopic (EIS) Studies. To gain further understanding of the differences in the electrochemical performances and polarization behaviors between the bare and the surface-modified samples, the samples were analyzed by electrochemical impedance spectroscopy at both third and 50th cycles. Before the EIS measurements, all the samples were charged to 50% state of charge (SOC) to reach an identical status. The EIS spectra of the bare and surface modified samples are compared in Figure 10. Each spectrum consists of two semicircles and a slope. According to the reaction mechanism of the 5 V spinel samples proposed by Alcántara et al.,[15] the first semicircle (at high-frequency region) is ascribed to lithium-ion diffusion through the surface layer, the second semicircle (at medium-to-low frequency region) is assigned to charge-transfer reaction, and the slope at the low-frequency region is attributed to lithium-ion diffusion in the bulk material.

On the basis of this mechanism, the equivalent circuit for the bare and surface-modified $LiMn_{1.42}Ni_{0.42}Co_{0.16}O_4$ samples is given in Figure 11. In this equivalent circuit, R_Ω refers the uncompensated ohmic resistance of the working electrode, R_s represents the resistance for lithium-ion diffusion in the surface layer (including SEI layer and surface modification layer), CPE_s is the constant phase-angle element depicting the nonideal capacitance of the surface layer, R_{ct} refers to charge transfer resistance, Z_w represents the Warburg impedance describing the lithium-ion diffusion in the bulk material, and CPE_{dl} is the constant phase-angle element depicting the nonideal capacitance of the double layer. Among these parameters, R_Ω and R_{ct} are two of the three components of R_P, whereas R_s and Z_w contribute to the third component R_d of R_P. Because the particle size and crystallographic structure are identical for the bare and the coated samples, it can be assumed that the lithium diffusion behavior in the bulk material is identical, i.e., the bare and the coated sample have the same Z_w value. Meanwhile, the value of R_Ω, which is given by the intersection of the first semicircle with the horizontal axis at very high frequency, is negligible for all samples (see Figure 10). Therefore, the difference between the R_P values of the bare and the coated samples should mainly arise from the differences in the R_s and R_{ct} values.

To elucidate the relationship of R_P to R_s and R_{ct}, we calculated the R_s, R_{ct}, ΔR_s (the increase in R_s on going from third to 50th cycle), ΔR_{ct} (the increase in R_{ct} on going from third to 50th cycle), $R_s + R_{ct}$, and $\Delta R_s + \Delta R_{ct}$ values for the bare and surface-modified $LiMn_{1.42}Ni_{0.42}Co_{0.16}O_4$, and the values are given in Table 2. By carefully examining the data, we can see that the trends in the R_{ct} values at third and 50th cycles and ΔR_{ct} value are similar to the trends in the rate capabilities at the third and 50th cycles and the rate capability retention in Figure 7 as well as the trends in the R_P values at third and 50th cycles and ΔR_P value in Figure 9. But for R_s, ΔR_s, $R_s + R_{ct}$, and $\Delta R_s + \Delta R_{ct}$, this kind of correlation is not so pronounced, especially for the surface-modified samples. The data reveal that (i) the charge-transfer reaction remains as a rate determining step in the discharge reaction of $LiMn_{1.42}Ni_{0.42}Co_{0.16}O_4$ in addition to the lithium-ion diffusion in the bulk material, (ii) the contribution of R_{ct} to the total polarization resistance R_P is much larger than that of R_s, and (iii) ΔR_P results mainly from ΔR_{ct} (considering that R_d remains constant during cycling).

Additionally, as seen in Figure 10 and Table 2, the ΔR_s and ΔR_{ct} values of the bare sample are much larger than those of the surface-modified samples, indicating that the surface chemistry of the surface-modified samples is much more stable compared to that of the bare sample. By further comparing the values of ΔR_s, we can see that ΔR_s increases in the order Al_2O_3-coated sample < ZnO-coated sample < Bi_2O_3-coated sample < $AlPO_4$-coated sample < bare sample, which is generally in the reverse order of capacity retention. The results suggest that the capacity fade is closely related to the increase in surface resistance.

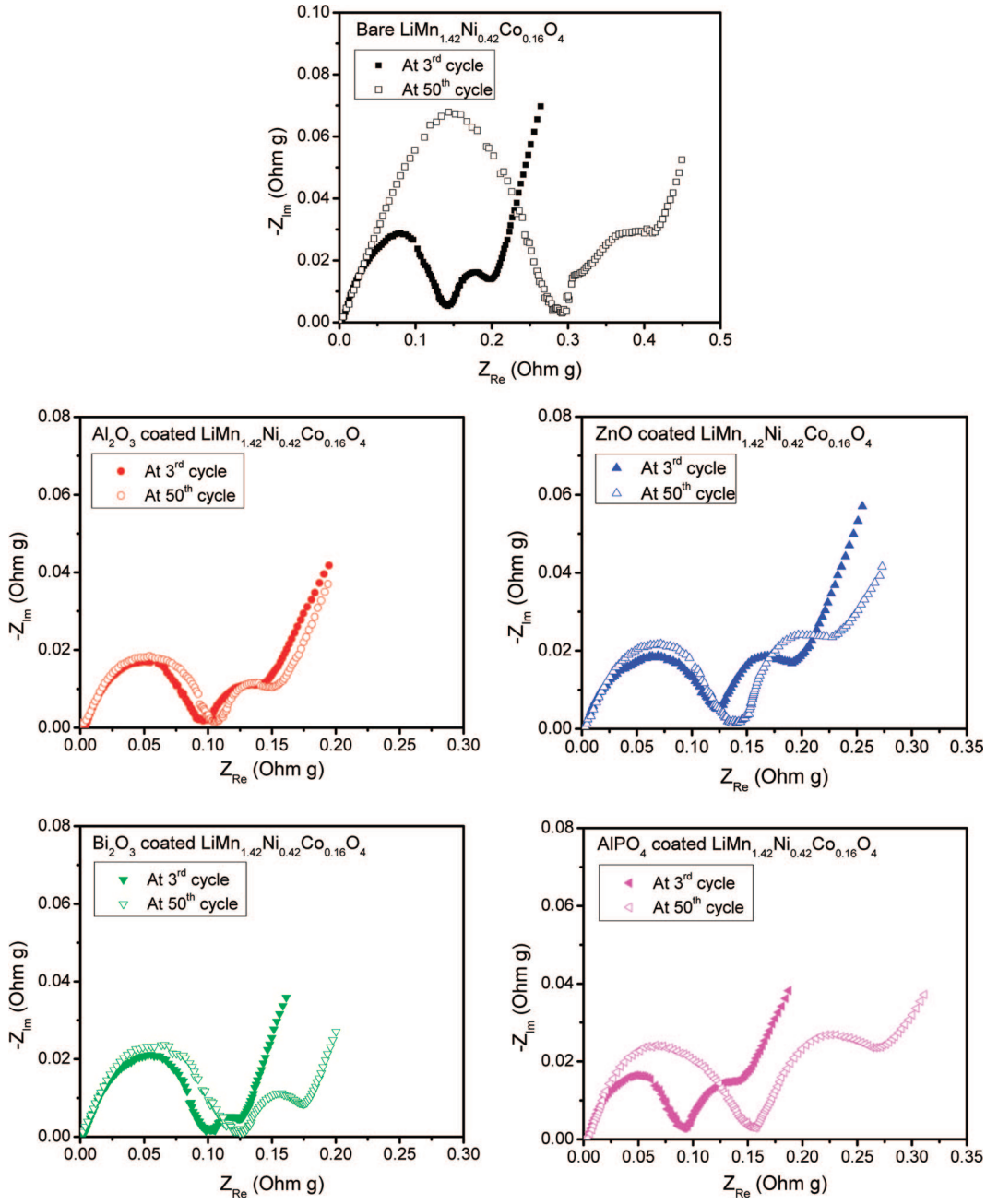

Figure 10. Electrochemical impedance spectra (EIS) of bare and 2 wt % Al_2O_3, ZnO, Bi_2O_3, and $AlPO_4$-coated $LiMn_{1.42}Ni_{0.42}Co_{0.16}O_4$ at 3rd cycle and 50th cycles.

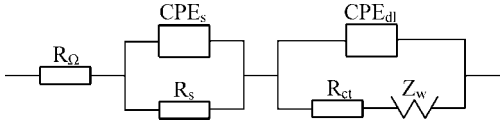

Figure 11. Equivalent circuit for the bare and surface-modified $LiMn_{1.42}Ni_{0.42}Co_{0.16}O_4$.

X-ray Photoelectron Spectroscopic (XPS) Studies. *Chemical States of the Surface Modification Layers before and after Cycling.* It is easy to envision that the differences in the electrochemical performances between the bare and the surface-modified samples could be due to protection of the cathode surface by the coated layers from direct contact with the electrolyte and a suppression of electrolyte decomposition at high operating voltages on the cathode surface. However, from the data presented above, we find that the electrochemical performances differ depending on the surface modifying materials. Therefore, it will be interesting to investigate the chemical states of the different surface modification layers.

Accordingly, Figure 12 shows the XPS spectra of the elements in various surface modification layers before and after 50 charge−discharge cycles. Panels a and b in Figure 12 show the Al 2p and P 2p peaks in the $AlPO_4$-modified sample. The Al 2p and P 2p peaks occur, respectively, at 74.7 and 134.3 eV before cycling, which are close to the Al 2p (74.5 eV) and P 2p (134.5 eV) binding energy values reported for the 400 °C annealed $AlPO_4$-coated $LiCoO_2$[44] and Al 2p (75.0 eV) and P 2p (134.4 eV) values reported

(44) Kim, B.; Kim, C.; Ahn, D.; Moon, T.; Ahn, J.; Park, Y.; Park, B. *Electrochem. Solid-State Lett.* **2007**, *10*, A32.

Table 2. Calculated Surface Resistance (R_s) and Charge Transfer Resistance (R_{ct}) Values at Different Cycles

	R_s (Ohm g)			R_{ct} (Ohm g)			$(\Delta R_s + \Delta R_{ct})$ (Ohm g)		
sample	at 3rd cycle	at 50th cycle	ΔR_s (Ohm g)	at 3rd cycle	at 50th cycle	ΔR_{ct} (Ohm g)	at 3rd cycle	at 50th cycle	$(\Delta R_s + \Delta R_{ct})$ (Ohm g)
bare $LiMn_{1.42}Ni_{0.42}Co_{0.16}O_4$	0.161	0.286	0.125	0.075	0.198	0.123	0.236	0.484	0.248
$AlPO_4$ coated $LiMn_{1.42}Ni_{0.42}Co_{0.16}O_4$	0.090	0.153	0.063	0.072	0.145	0.073	0.162	0.298	0.136
Al_2O_3-coated $LiMn_{1.42}Ni_{0.42}Co_{0.16}O_4$	0.095	0.106	0.011	0.059	0.068	0.009	0.154	0.174	0.020
ZnO-coated $LiMn_{1.42}Ni_{0.42}Co_{0.16}O_4$	0.123	0.139	0.016	0.091	0.110	0.019	0.214	0.249	0.035
Bi_2O_3-coated $LiMn_{1.42}Ni_{0.42}Co_{0.16}O_4$	0.100	0.125	0.025	0.038	0.053	0.015	0.138	0.178	0.040

for $AlPO_4$.[31] However, the peak positions are different from those reported (73.3 eV for Al 2p peak and 133.2 eV for P 2p peak) for the 700 °C annealed $AlPO_4$-coated $LiCoO_2$.[31] The data indicate that the annealing temperature is a critical factor in determining the chemical states of the $AlPO_4$ surface-modification layer. The Al 2p and P 2p peaks occur, respectively, at 74.9 and 134.5 eV after 50 cycles in panels a and b in Figure 12, which are close to the values found before cycling.

Figure 12c shows the Al 2p spectra of the Al_2O_3 modified sample before and after 50 cycles. The Al 2p peak remains unchanged at 73.6 eV before and after 50 cycles. The value is lower than that observed in Al_2O_3 (74.2 eV),[45] but is close to that reported for $LiAlO_2$ (73.4 eV).[31] The data suggest

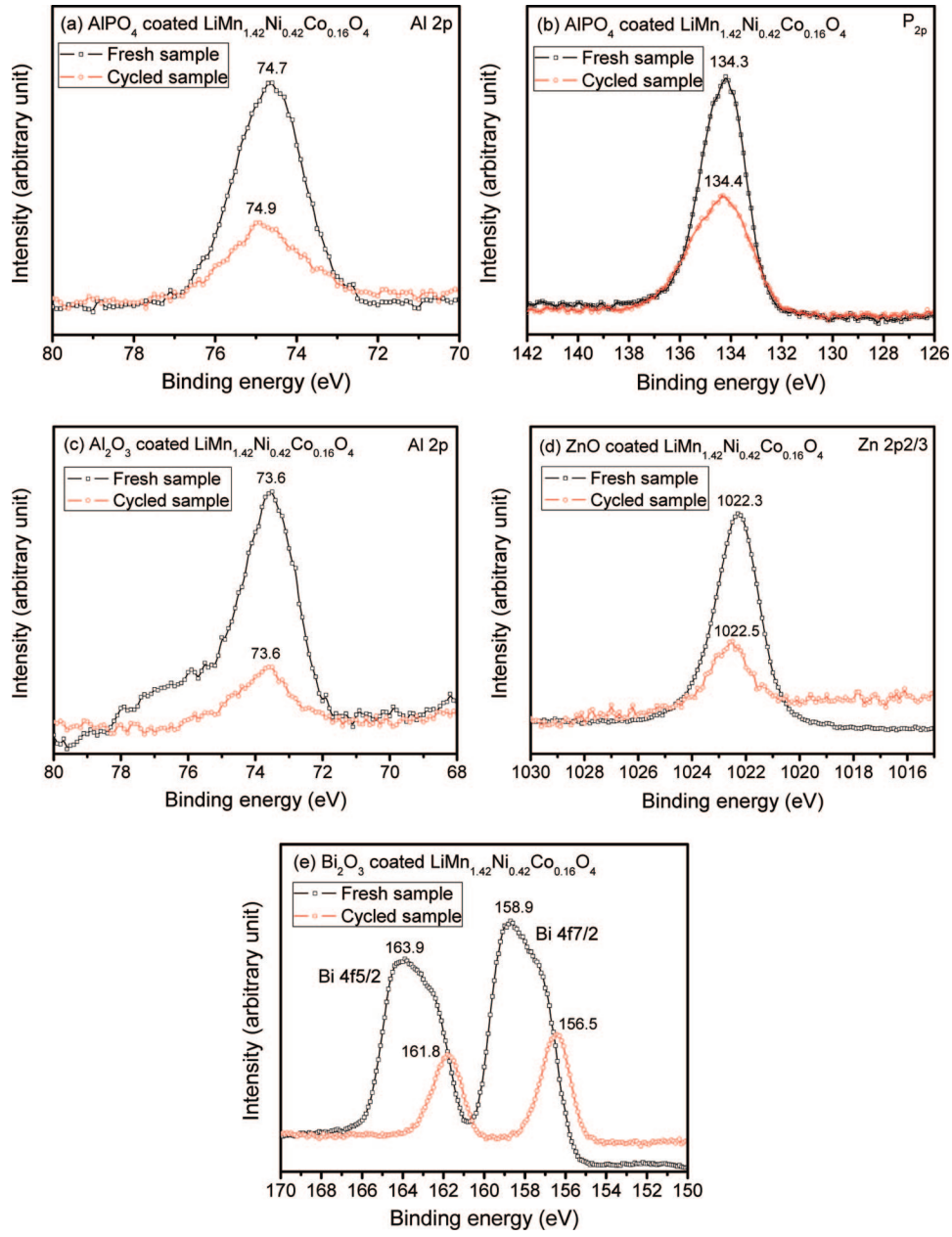

Figure 12. Comparison of the XPS spectra of surface-modified $LiMn_{1.42}Ni_{0.42}Co_{0.16}O_4$ samples: (a) Al 2p spectrum of 2 wt % $AlPO_4$-coated sample, (b) P 2p spectrum of 2 wt % $AlPO_4$-coated sample, (c) Al 2p spectrum of 2 wt % Al_2O_3-coated sample, (d) Zn 2p spectrum of 2 wt % ZnO-coated sample, and (e) Bi 4f spectrum of 2 wt % Bi_2O_3-coated sample.

that Al_2O_3 might have reacted with the cathode surface during the annealing process to form $LiAlO_2$ on the surface.

Figure 12d shows the Zn $2p_{3/2}$ spectra of the ZnO modified sample before and after 50 cycles. The Zn $2p_{3/2}$ peak occurs at 1022.3 and 1022.5 eV, respectively, before and after 50 cycles. This value is similar to that found in ZnO,[46] indicating that the chemical state of ZnO is unchanged after annealing and after cycling.

Figure 12e shows the Bi 4f spectra of the Bi_2O_3 modified sample before and after 50 cycles. Significant shifts in the binding energies of the Bi $4f_{5/2}$ and $4f_{7/2}$ peaks were observed after cycling. Specifically, the Bi $4f_{5/2}$ peak shifts from 163.9 to 161.8 eV and the Bi $4f_{7/2}$ peak shifts from 158.9 to 156.5 eV after 50 cycles. Because the peaks at 163.9 and 158.9 eV correspond to Bi_2O_3 and the peaks at 161.8 and 156.5 eV correspond to Bi metal,[46] the data reveal that Bi_2O_3 is reduced to Bi metal during cycling. This result is consistent with the finding of Bervas et al.[47] that Bi_2O_3 starts to be reduced into Bi metal at the very beginning of lithium intercalation (discharge) process.

It should be noted that although well-defined photoemission peaks could be obtained with a single time scan before cycling, each element needed to be scanned 3−5 times after 50 cycles to obtain meaningful peak intensities. This may be related to the possible development of solid-electrolyte interfacial (SEI) layers on the surface of the samples during cycling.

Depth Profile Analysis. The ideal SEI layer should be thin and allow lithium-ion conduction.[48] However, electrolyte is easy to decompose on the surface of the 5 V spinel cathode because of the higher operating voltage, resulting in the formation of thick SEI layers. Theoretically, the thickness of the SEI layer can be calculated from a depth profile analysis of the SEI layer.[49] However, in reality, it is hard to determine the sputtering rate of the SEI layer, resulting in difficulties to obtain the absolute value of the thickness of the SEI layer. Nevertheless, the thickness of different SEI layers could be semiquantitatively compared on the basis of the sputtering time, if the composition and microstructure of the SEI layers do not differ significantly. LiF has been reported to be a major component of SEI layers.[49−51] Accordingly, we analyzed the depth profiles of LiF on the bare and surface-modified samples.

Figure 13 shows the F 1s photoemission peaks of all samples at various sputtering times. The main peaks at ~685 eV are assigned to LiF, whereas the peaks above 687 eV are assigned to $LiPF_6$, Li_xPF_y, and Li_xPOF_y formed by a reaction of $LiPF_6$ salt.[48] In each case in Figure 13, the intensity of the LiF peak increased sharply to the maximum value after 10 s, indicating possibly the formation of a thin layer in contact with the ambient, and then decreased gradually with a further increase in sputtering time. For each sample, the concentration of LiF at different depths (i.e. after different sputtering time) was normalized with respect to its maximum value, and the normalized concentration of LiF is plotted as a function of sputtering time in Figure 14. As seen, the concentration of LiF at a given depth or after a given sputtering time varies significantly on going from one sample to another. In other words, it takes different amounts of sputtering time to see a specific concentration of LiF. For example, to see a LiF concentration of 60% of the maximum value, it takes 580, 50, 80, 110, and 150 s, respectively, for the bare, Al_2O_3, ZnO, Bi_2O_3, and $AlPO_4$-coated $LiMn_{1.42}Ni_{0.42}Co_{0.16}O_4$ samples. The results imply that the SEI layer on the bare sample is much thicker than that on the surface-modified samples, and especially the Al_2O_3 coating is the most effective in suppressing of the development of the SEI layer. The thickness of the SEI layer decreases in the order bare sample > $AlPO_4$-coated sample > Bi_2O_3-coated sample > ZnO-coated sample > Al_2O_3-coated sample, which agrees well with the decreasing order of ΔR_s found in the EIS study (Table 2). This indicates that ΔR_s is due to the development of the SEI layer.

Capacity Fade Mechanism of 5 V Spinel. As pointed out earlier, the capacity fade is closely related to the increase in surface resistance ΔR_s, which is due to the development of the SEI layer. Also, the SEI layer is known to be highly resistive. Therefore, we can say that the development of the SEI layer is one of the reasons for the capacity fade of 5 V spinels during charge−discharge cycles.

Furthermore, the $LiFP_6$ salt in the electrolyte is electrochemically unstable at high voltages,[52] and the oxidation of PF_6^-, occurring at around 5 V vs Li/ Li^+, proceeds according to the following reactions[53]

$$PF_6^- - e \rightarrow PF_6^\bullet \rightarrow PF_5 + F^\bullet \quad \text{(i)}$$

$$F^\bullet \xrightarrow{H\ -\ \text{Abstraction}} HF \quad \text{(ii)}$$

where trace amounts of H_2O present in the electrolyte serves as the source of proton of H-abstraction. The HF formed can attack the active material surface[54] by the following autocatalytic corrosion reaction

$$LiM_xO_y + HF \rightarrow LiF + M^{n+} + F^- + H_2O \quad \text{(iii)}$$

$$H_2O + LiPF_6 \rightarrow LiF + POF_3 + 2HF \quad \text{(iv)}$$

where M refers to transition metal. The high operating voltage of the 5 V spinel cathodes can accelerate the formation of HF and the increased concentration of HF can enhance the corrosion rate of the active material and the deposition rate of SEI components such as LiF and LiOH

(45) Liu, J.; Yang, Y.-F.; Yu, P.; Li, Y.; Shao, H.-X. *J. Power Sources* **2007**, *161*, 1435.
(46) Moulder, J. F.; Stickle, W. F.; Sobol, P. E.; Bomben, K. D. *Handbook of X-ray Photoelectron Spectroscopy*; Perkin-Elmer Corporation: Eden Prairie, MN, 1992.
(47) Bervas, M.; Klein, L. C.; Amatuccia, G. G. *J. Electrochem. Soc.* **2006**, *153*, A159.
(48) Lu, M.; Cheng, H.; Yang, Y. *Electrochim. Acta* **2008**, *53*, 3539.
(49) Andersson, A. M.; Henningson, A.; Siegbahn, H.; Jansson, U.; Edstrom, K. *J. Power Sources* **2003**, *119−121*, 522.
(50) Andersson, A. M.; Edstrom, K. *J. Electrochem. Soc.* **2001**, *148*, A1100.
(51) Edstrom, K.; Gustafsson, T.; Thomas, J. O. *Electrochim. Acta* **2004**, *50*, 397.
(52) Xu, K. *Chem. Rev.* **2004**, *104*, 4303.
(53) Koch, V. R.; Dominey, L. A.; Nanjundiah, C.; Ondrechen, M. J. *J. Electrochem. Soc.* **1996**, *143*, 798.
(54) Myung, S.; Izumi, K.; Komaba, S.; Sun, Y.; Yashiro, H.; Kumagai, N. *Chem. Mater.* **2005**, *17*, 3695.

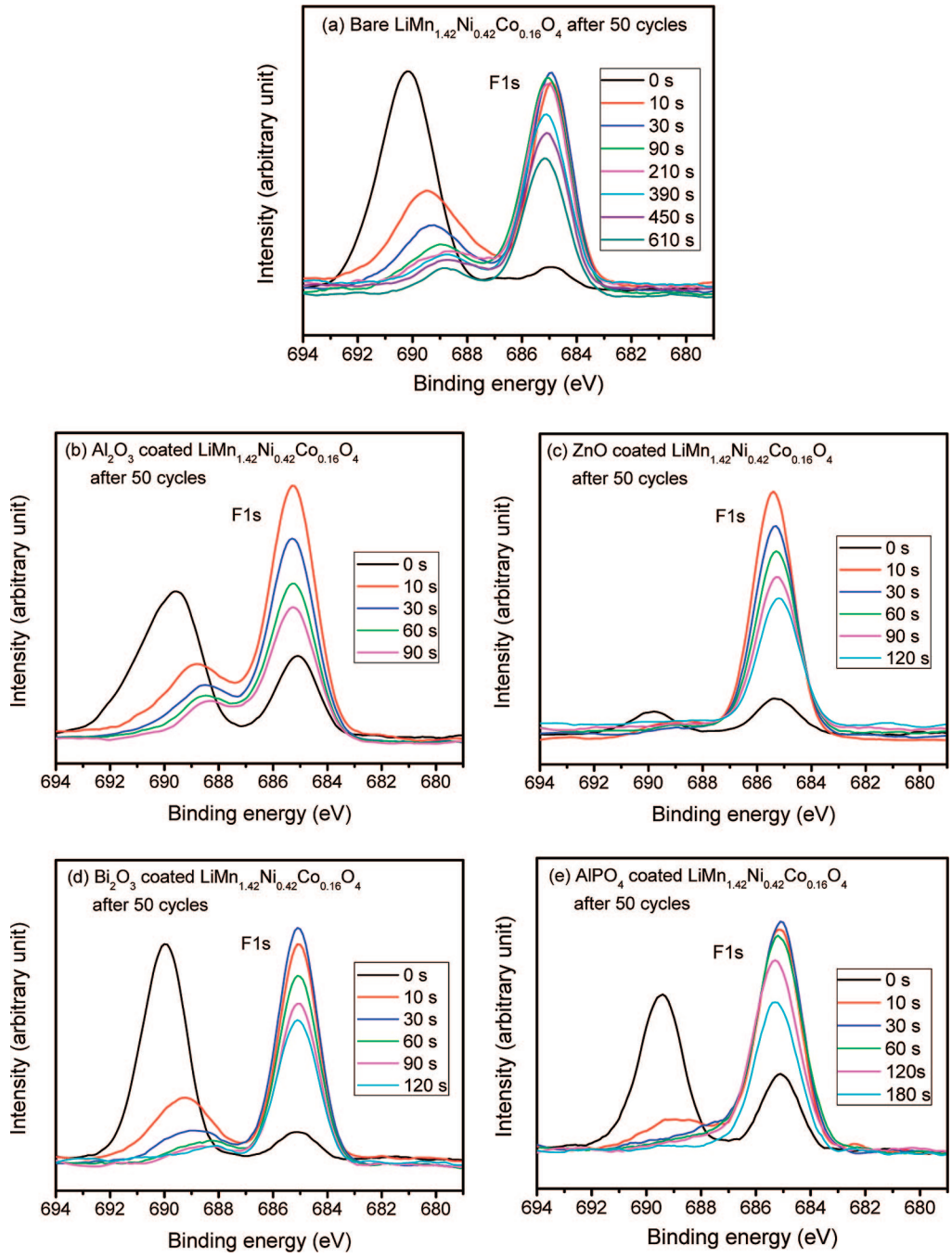

Figure 13. F 1s XPS spectra of the bare and surface-modified samples at different sputtering times: (a) bare, (b) 2 wt % Al_2O_3-coated, (c) 2 wt % ZnO-coated, (d) 2 wt %-Bi_2O_3 coated, and (e) 2 wt % $AlPO_4$-coated $LiMn_{1.42}Ni_{0.42}Co_{0.16}O_4$ after 50 charge−discharge cycles.

on cathode surface. Thus, the enhanced corrosion by HF can lead to capacity fade and a thicker SEI layer.

Role of SEI Layer on Electrochemical Performance. The fact that the SEI layer on the bare $LiMn_{1.42}Ni_{0.42}Co_{0.16}O_4$ is much thicker than that on the surface-modified sample (Figure 14) indicates that Al_2O_3, ZnO, Bi_2O_3, and $AlPO_4$ modifications significantly slow down the kinetics of the electrolyte decomposition reaction at the interface between the electrolyte and the active cathode material. As a result, corrosion of the active cathode material is greatly reduced and the cycling performance is significantly improved.

As mentioned earlier, charge-transfer reaction is one of the rate-determining steps of the lithium insertion/extraction process. The rate of charge-transfer reaction depends not only on the rate constant K^0 and electrode potential but also on the rate of Li^+ ion and electron transport on to or out of the surface of the active material. The SEI layer formed with the $LiFP_6$ electrolyte solution is reported to be less conductive because the major SEI component LiF is highly resistive to both Li^+ ion and electron transport.[55] Thus, the low charge-transfer rate and the poor rate capability of the bare $LiMn_{1.42}Ni_{0.42}Co_{0.16}O_4$ appear to originate from the thick SEI layer, and the improved charge-transfer rate and rate capability of the surface-modified samples is due to the reduction

(55) Aurbach, D.; Gamolsky, K.; Markovsky, B.; Salitra, G.; Gofer, Y.; Heider, U.; Oesten, R.; Schmidt, M. *J. Electrochem. Soc.* **2000**, *147*, 1322.

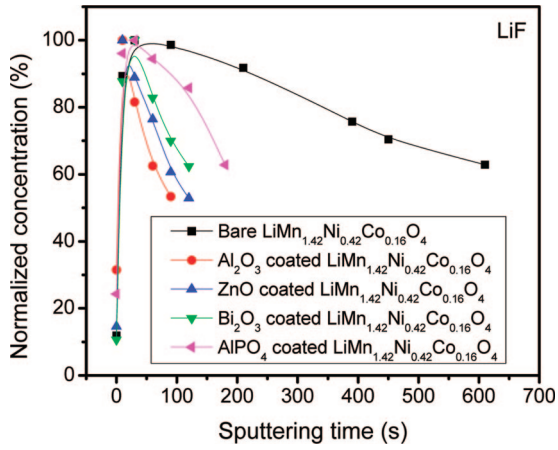

Figure 14. Variations of normalized LiF concentration with sputtering time for the bare and 2 wt % Al_2O_3, ZnO, Bi_2O_3, and $AlPO_4$-coated $LiMn_{1.42}Ni_{0.42}Co_{0.16}O_4$ after 50 charge−discharge cycles.

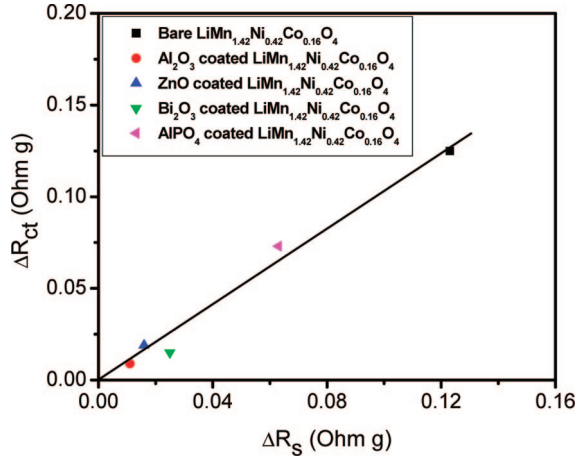

Figure 15. Relationship between ΔR_{ct} and ΔR_s of the bare and 2 wt % Al_2O_3, ZnO, Bi_2O_3, and $AlPO_4$-coated $LiMn_{1.42}Ni_{0.42}Co_{0.16}O_4$.

in the thickness of the SEI layer. To further confirm the relationship between the SEI layer and rate capability, we plot ΔR_{ct} versus ΔR_s in Figure 15. As seen, ΔR_{ct} increases linearly with increasing ΔR_s, confirming that the thickness of the SEI layer plays an important role in determining the rate capability.

Role of Surface Modification Layer Microstructure on Electrochemical Performance. The microstructure of the surface modification layer plays an important role in determining the electrochemical performances of the active material.[31] In this study, the $AlPO_4$-coated $LiMn_{1.42}Ni_{0.42}Co_{0.16}O_4$ sample shows a discrete and dense surface modification layer as seen in Figure 3. This means a small portion of the active material may be directly exposed to the electrolyte. During the initial number of cycles, the SEI layer is less developed, and the uncovered surface may provide the effective sites for the charge-transfer reaction, which leads to a small R_{ct} and good rate capability. However, as the cycle number increases, the SEI layer is intensively developed on the uncovered surface and the thick and less-conductive SEI layer increases R_s and R_{ct} and degrades the rate capability. Also, the slow kinetics of the Li^+ ion diffusion through the $AlPO_4$ modification layer may also contribute to the poor rate capability of the $AlPO_4$-coated $LiMn_{1.42}Ni_{0.42}Co_{0.16}O_4$ after a long cycling time. Because the uncovered surface is only a small portion, the capacity decay of $AlPO_4$-coated $LiMn_{1.42}Ni_{0.42}Co_{0.16}O_4$ is not serious during 50 cycles. In contrast to the $AlPO_4$ coating, the surface modification layers are all continuous and more porous in the case of Al_2O_3, ZnO, and Bi_2O_3-coated samples. The continuous modification layer can effectively protect the active material from "electrolyte attack" and suppress the fast development of the SEI layer. Thus the Al_2O_3, ZnO, and Bi_2O_3-coated $LiMn_{1.42}Ni_{0.42}Co_{0.16}O_4$ samples exhibit good cycling performances. Also, the thin SEI layer results in smaller R_s and R_{ct}, rendering good rate capability even after 50 cycles.

Role of Surface Modification Layer Composition on Electrochemical Performance. Although the surface-modified samples exhibit better electrochemical performance than the bare sample, they also differ significantly in their performance depending on the coating material. Among the four surface modifications investigated here, both ZnO and $AlPO_4$ remain unchanged during the annealing and electrochemical cycling processes. Both ZnO and $AlPO_4$ are neither good lithium-ion conductors nor good electronic conductors. Therefore, both the ZnO and $AlPO_4$ coating layers act only as an inert protection shell between the active cathode surface and the electrolyte. On the other hand, Al_2O_3 reacts with the surface of $LiMn_{1.42}Ni_{0.42}Co_{0.16}O_4$ during the annealing process and forms $LiAlO_2$ that exhibit good lithium-ion conductivity.[56] Therefore, "Al_2O_3" modification layer acts as both a protection shell and as a fast lithium-ion diffusion channel, rendering both excellent cycling performance and good rate capability for the Al_2O_3-coated $LiMn_{1.42}Ni_{0.42}Co_{0.16}O_4$. Similarly, Bi_2O_3 is reduced on the cathode surface during electrochemical cycling to metallic Bi, which is an electronic conductor. Thus, the "Bi_2O_3" modification layer acts both as a protection shell and as a fast electron transfer channel, rendering both excellent rate capability and good cycling performance for the Bi_2O_3-coated $LiMn_{1.42}Ni_{0.42}Co_{0.16}O_4$. However, the cycling performance of the Bi_2O_3-coated $LiMn_{1.42}Ni_{0.42}Co_{0.16}O_4$ is not as good as that of the Al_2O_3-coated sample. This might be due to the microstructural changes of the Bi_2O_3 modification layer during the reduction process.

Conclusions

An electrostatic self-assembly method has been employed to modify the surface of the 5 V spinel cathode $LiMn_{1.42}Ni_{0.42}Co_{0.16}O_4$ with 2 wt % nanosize Al_2O_3, ZnO, Bi_2O_3, and $AlPO_4$. The surface modified samples with a much more stable surface chemistry suppress the development of SEI layer and thereby improve the electrochemical performances significantly compared to the bare $LiMn_{1.42}Ni_{0.42}Co_{0.16}O_4$. However, the surface modified samples also differ among themselves in their electrochemical performances due to the different functions of the four surface modification materials investigated. Specifically, although both the ZnO and $AlPO_4$ modification layers act only as a protection shell between the active cathode material surface and the elec-

(56) Myung, S. T.; Kumagai, N.; Komaba, S.; Chung, H. T. *Solid State Ionics* **2001**, *139*, 47.

trolyte, the Al_2O_3 and Bi_2O_3 modification layers offer, respectively, fast lithium-ion diffusion channel and fast electron-transfer channel, in addition to acting as a protection shell.

The study demonstrates that surface modifications may prove to be a viable approach to utilize the high-voltage cathodes in lithium-ion cells. The data presented here illustrate the criteria for choosing appropriate surface modification materials that can maximize the overall electrochemical performance. Although surface modification with materials like the ones investigated here may generally be perceived to impede the electron and lithium-ion transport and thereby degrade the rate capability, the suppression of undesired SEI layer formation along with favorable lithium-ion and electron-diffusion pathways results in enhanced rate capability and cyclability.

Acknowledgment. This work was supported by the Office of Vehicle Technologies of the U.S. Department of Energy under Contract DE-AC02−05CH11231. The authors thank Drs. Y. M. Sun, H. Celio, and L. Xiong for their assistance with the XPS and TEM data collection.

CM9000043